

# Particle-scale reversibility in athermal particulate media below jamming

Carl F. Schreck<sup>1,2</sup>, Robert S. Hoy<sup>3</sup>, Mark D. Shattuck<sup>4,1</sup>, and Corey S. O’Hern<sup>1,2,5</sup>

<sup>1</sup>*Department of Mechanical Engineering & Materials Science,  
Yale University, New Haven, Connecticut 06520-8260, USA*

<sup>2</sup>*Department of Physics, Yale University, New Haven, Connecticut 06520-8120, USA*

<sup>3</sup>*Department of Physics, University of South Florida, Tampa, Florida 33620, USA*

<sup>4</sup>*Benjamin Levich Institute and Physics Department,*

*The City College of the City University of New York, New York, New York 10031, USA and*

<sup>5</sup>*Department of Applied Physics, Yale University, New Haven, Connecticut 06520-8120, USA*

We perform numerical simulations of athermal repulsive frictionless disks and spheres in two and three spatial dimensions undergoing cyclic quasi-static simple shear to investigate particle-scale reversible motion. We identify three classes of steady-state dynamics as a function of packing fraction  $\phi$  and maximum strain amplitude per cycle  $\gamma_{\max}$ . Point-reversible states, where particles do not collide and exactly retrace their intra-cycle trajectories, occur at low  $\phi$  and  $\gamma_{\max}$ . Particles in loop-reversible states undergo numerous collisions and execute complex trajectories, but return to their initial positions at the end of each cycle. Loop-reversible dynamics represents a novel form of self-organization that enables reliable preparation of configurations with specified structural and mechanical properties over a broad range of  $\phi$  from contact percolation to jamming onset at  $\phi_J$ . For sufficiently large  $\phi$  and  $\gamma_{\max}$ , systems display irreversible dynamics with nonzero self-diffusion.

PACS numbers: 83.80.Fg, 61.43.-j, 63.50.Lm, 62.20.-x

In equilibrium thermal systems, reversible processes are imagined as transitions from one thermodynamic microstate to another with no change in free energy. For example, thermal fluctuations in high-temperature fluids give rise to particle motions that yield only very small changes in entropy. However, finite deformations of supercooled liquids and amorphous solids, upon reversal of the strain, can produce microscopically *irreversible* motion, such as collective particle rearrangements [1], anelasticity, and plastic flow [2]. The identification of topological defects in crystalline materials is straightforward, whereas it is much more difficult to identify particle-scale motion that gives rise to plasticity in amorphous materials [3].

Granular materials, foams, and other athermal particulate media are highly dissipative, and therefore must be driven to induce particle motion. Experimental studies of granular media have shown macroscale reversibility of the packing fraction during cyclic shear [4] and vibration [5]. Since these systems are far from thermal equilibrium, one might assume that they do not display *microscale* reversible motion when subjected to cyclic driving. Experimental and computational studies of 2D foams have identified both reversible and irreversible T1 bubble neighbor switching events during cyclic shear [6]. Researchers have also shown that motion of individual particles transitions from reversible to irreversible beyond a density-dependent critical strain, which decreases with increasing packing fraction, in cyclically sheared suspensions [7, 8].

An important open question is whether athermal particulate media can undergo completely reversible motion due to inter-grain collisions when subjected to cyclic loading. We address this question by performing numerical simulations of frictionless granular materials in two and three spatial dimensions undergoing quasistatic

cyclic simple shear [9] over a wide range of packing fraction  $\phi$  and shear strain amplitude  $\gamma_{\max}$ . We identify two classes of grain-scale reversible motion, point and loop (which are stable to finite perturbations). For point-reversible dynamics, particles do not collide during the forward cycle, and thus they exactly retrace their trajectories upon reversal. In contrast, particle collisions occur frequently during loop-reversible dynamics, but the system self-organizes so that particles return to the same positions at the beginning of each cycle, despite complex particle motion during the cycle. We map out the ‘dynamical phase diagram’ as a function of  $\phi$  and  $\gamma_{\max}$ . The system transitions from point- to loop-reversible and then from loop-reversible to irreversible (with nonzero self-diffusion) dynamics with increasing  $\phi$  and  $\gamma_{\max}$ . We show that the time evolution toward steady-state point- and loop-reversible behavior can be collapsed onto a universal scaling function with power-law scaling at short and intermediate times, and exponential decay at long times.

We perform numerical studies of  $N$  athermal disks and spheres undergoing quasi-static, cyclic simple shear in 2D and 3D at constant  $\phi$  using shear-periodic boundary conditions in square or cubic cells [11]. Particles interact via the pairwise, purely repulsive linear spring potential

$$V(r_{ij}) = \frac{\epsilon}{2} \left(1 - \frac{r_{ij}}{\sigma_{ij}}\right)^2 \Theta(\sigma_{ij} - r_{ij}), \quad (1)$$

where  $r_{ij}$  is the center-to-center separation between particles  $i$  and  $j$ ,  $\Theta(x)$  is the Heaviside step function,  $\sigma_{ij} = (\sigma_i + \sigma_j)/2$ , and  $\sigma_i$  is the diameter of particle  $i$ . We focus on bidisperse particle size distributions, *i.e.* 50-50 mixtures by number with diameter ratio  $\sigma_l/\sigma_s = 1.4$ , to frustrate crystallization during shear [12]. We consider system sizes from  $N = 32$  to 512 to assess finite size ef-

fects for packing fractions below and near the onset of jamming ( $\phi_J \sim 0.84$  [10] in 2D and  $\sim 0.65$  [13] in 3D).

The particles are initially placed randomly in the simulation cell at packing fraction  $\phi$  and then relaxed using conjugate gradient energy minimization [12]. We apply simple shear strain by shifting each particle horizontally

$$x_{n,k+1}^i = x_{n,k}^i + \Delta\gamma y_{n,k}^i, \quad (2)$$

in increments of  $\Delta\gamma = 10^{-3}$ , where  $x_{n,k}^i$  and  $y_{n,k}^i$  are coordinates of particle  $i$  at the  $k$ th step of strain cycle  $n$  [14]. After each strain step, we minimize the total potential energy at fixed shear strain,  $\gamma_k = k\Delta\gamma$  for the forward or  $\gamma_k = 2\gamma_{\max} - k\Delta\gamma$  for the reverse part of the cycle. This process is repeated for up to  $n = 10^6$  cycles.

During the simulations, we measure the single cycle mean-square displacement (at step  $k = 0$  for each cycle)

$$\begin{aligned} \Delta r_1^2(n) = (N\sigma_s^2)^{-1} \sum_i & \left( (X_{n,0}^i - X_{n+1,0}^i)^2 \right. \\ & \left. + (Y_{n,0}^i - Y_{n+1,0}^i)^2 + (Z_{n,0}^i - Z_{n+1,0}^i)^2 \right) \quad (3) \end{aligned}$$

and arc length

$$\begin{aligned} L^2(n) = (N\sigma_s^2)^{-1} \sum_i & \left( \sum_k [(X_{n,k+1}^i - X_{n,k}^i)^2 \right. \\ & \left. + (Y_{n,k+1}^i - Y_{n,k}^i)^2 + (Z_{n,k+1}^i - Z_{n,k}^i)^2]^{1/2} \right)^2 \quad (4) \end{aligned}$$

versus  $n$ , where  $X_{n,k}^i = x_{n,k}^i - \gamma_k y_{n,k}^i$ ,  $Y_{n,k}^i = y_{n,k}^i$ , and  $Z_{n,k}^i = z_{n,k}^i$  are the non-affine displacements of particle  $i$  after subtracting off the affine contribution. The long-time dynamics are either reversible or irreversible depending on  $\phi$  and  $\gamma_{\max}$ . We quantify the steady-state behavior by measuring  $\Delta r_1^2(n)$  and  $L^2(n)$  of the intra-cycle particle trajectories.

Particles in point-reversible systems organize to avoid collisions. At long times, no collisions take place, and  $L(n) = \Delta r_1(n) = 0$ , or more aptly, they fall below small numerical thresholds, *e.g.*  $\Delta r_1(n) < \tau_r = 5 \times 10^{-4}$  and  $L(n) < \tau_L = 10^{-8}$ . The values of  $\tau_r$  and  $\tau_L$  do not qualitatively affect our results as long as they are sufficiently small. Particle motions for point-reversible systems are affine and in the direction of the imposed affine shear (Fig. 1 (a)). Thus, the non-affine tracks of each particle are zero (Fig. 1 (d)).

In *loop-reversible* systems, particle collisions occur frequently, but the system self-organizes so that particles return to the same positions at the start of each cycle. Since collisions between particles occur,  $L(n) > 0$ , but  $\Delta r_1(n) = 0$  (*i.e.* below  $\tau_r$ ). Particle trajectories (Fig. 1 (b)) and non-affine displacements (Fig. 1 (e)) trace out complex paths, yet all particles end up in the same locations at the beginning of each new cycle, *i.e.*  $X_{n+1,0}^i = X_{n,0}^i$  and  $Y_{n+1,0}^i = Y_{n,0}^i$  in 2D. Thus, particle trajectories form closed loops in configuration space. We focus on period one loop-reversible systems, but multi-period dynamics are also found. Particle trajectories are

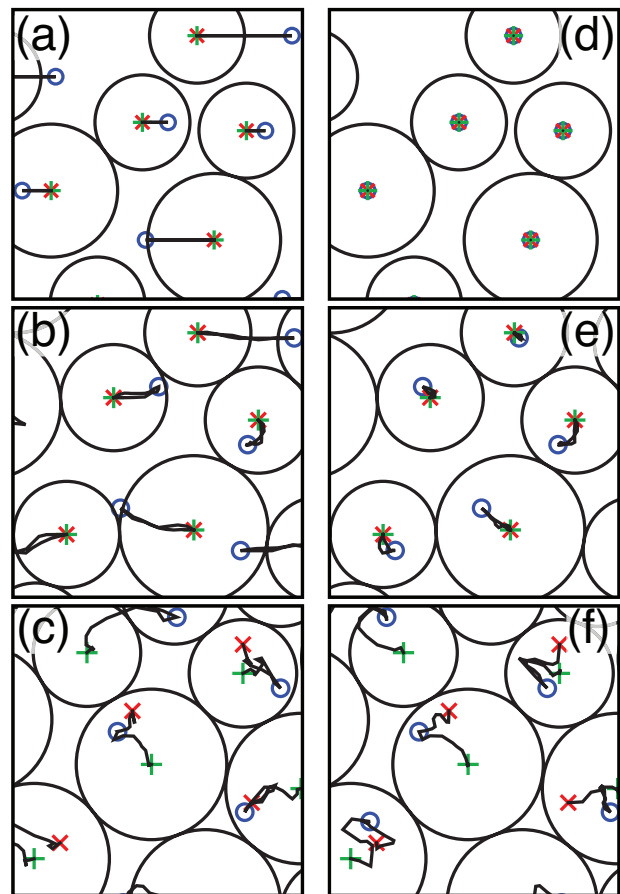


FIG. 1: (color online) Particle tracks (solid lines) in a small window of a  $N = 128$  system of bidisperse disks undergoing (a) point-reversible, (b) loop-reversible, and (c) irreversible behavior during cyclic simple shear. Panels (d), (e), and (f) show the disks' tracks in panels (a), (b), and (c), respectively, after subtracting off the affine motion. The systems in (a) and (d) correspond to  $\phi = 0.64$  and  $\gamma_{\max} = 0.8$ , (b) and (e) to  $\phi = 0.8$  and  $\gamma_{\max} = 0.8$ , (c) and (f) to  $\phi = 0.82$  and  $\gamma_{\max} = 0.8$ . Plus, circles, and crosses mark the beginning, middle, and end of the particle tracks, and particle outlines correspond to the beginning of the cycle.

elongated in the direction of affine displacement, whereas nonaffine displacements are more compact.

Particles in systems undergoing *irreversible* dynamics do not return to their original positions at the beginning of each new cycle, *e.g.*  $X_{n+1,0}^i \neq X_{n,0}^i$  and  $Y_{n+1,0}^i \neq Y_{n,0}^i$  in 2D. (Figs. 1 (c) and (f).) Irreversible systems have nonzero  $\Delta r_1(n)$  and  $L(n)$  (*i.e.*  $L(n) > \tau_L$  and  $\Delta r_1(n) > \tau_r$ ). Systems can be “transient” irreversible in time and evolve into point- or loop-reversible systems, or steady-state irreversible and remain irreversible in the large-cycle limit with nonzero self-diffusion.

The steady-state “dynamical phase diagram” in Fig. 2 (a) for cyclically sheared athermal disks shows point- and loop-reversible, as well as irreversible regimes versus  $\phi$  and  $\gamma_{\max}$  [14]. Point-reversible systems occur at

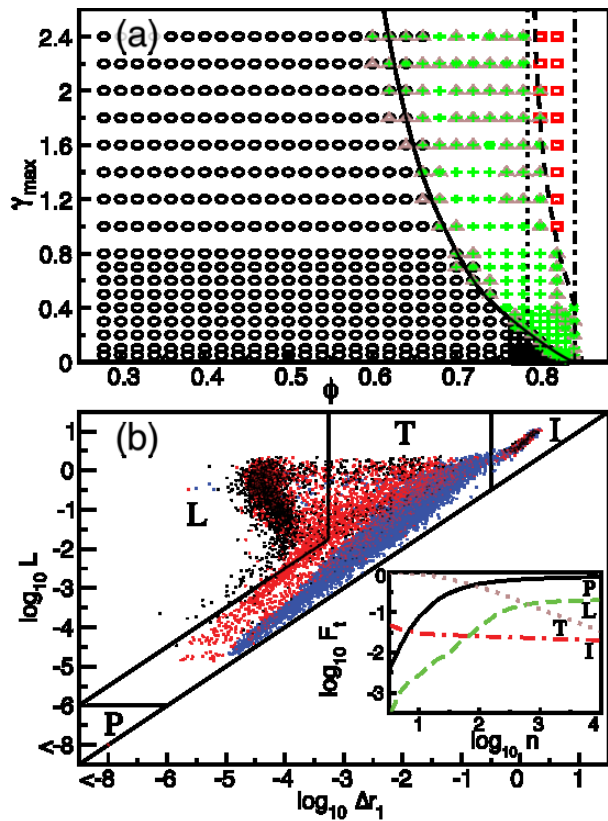


FIG. 2: (color online) (a) “Dynamical phase diagram” for  $N = 128$  bidisperse disks after  $n = 10^4$  cycles showing point-reversible (circles), period-one (pluses) or multi-period (crosses) loop-reversible, and transient (triangles) or steady-state (squares) irreversible dynamics versus  $\gamma_{\max}$  and  $\phi$ . The solid and dashed lines indicate  $\phi_L(\gamma_{\max})$  and  $\phi_I(\gamma_{\max})$ , the boundaries between point- and loop-reversible dynamics and between loop-reversible and irreversible dynamics, respectively. The vertical dotted and dot-dashed lines define  $\phi_R = 0.785$  and  $\phi_J \approx 0.84$ . (b) Intra-cycle mean-square displacement  $\Delta r_1$  versus arc-length  $L$  after  $n = 10$  (blue),  $3 \times 10^2$  (red), and  $10^4$  (black) cycles. The regions labeled  $P$ ,  $L$ ,  $T$ , and  $I$  define point-reversible, loop-reversible, transient irreversible, and steady-state irreversible dynamics, respectively. The  $P$ -region extends from  $L = \Delta r_1 = 10^{-6}$  to  $10^{-16}$  (not shown). The dashed boundaries indicate  $\Delta r_1 = \tau_r$ ,  $\Delta r_1 = 0.3\sigma_s$ ,  $L = \tau_L$ ,  $L = 30\Delta r_1$ , and  $L = \Delta r_1$  discussed in the main text. The inset shows the fraction  $F_t$  of systems in (a) categorized as point-reversible (solid), loop-reversible (dashed), transient irreversible (dotted), and irreversible (dot-dashed) dynamics versus  $n$ . Similar data for 3D systems is shown in Supplementary Material.

low  $\phi$  and  $\gamma_{\max}$ , whereas irreversible systems occur for  $\phi \gtrsim \phi_J$ . At intermediate packing fractions between roughly contact percolation [10] and jamming onset, *e.g.*  $0.6 \lesssim \phi \lesssim 0.84$  in 2D, loop-reversible systems are found. The boundary between point- and loop-reversible systems is  $\gamma_{\max} \sim A(\phi)(\phi_J - \phi)^\lambda \Theta(\phi_J - \phi)$ , where  $A(\phi)$  depends weakly on  $\phi$  and  $\lambda \sim 1.2 \pm 0.1$  for  $\phi \rightarrow \phi_J$

and  $2.2 \pm 0.2$  for  $\phi \ll \phi_J$ . Over a finite number of cycles (*i.e.*  $n < 10^4$  in Fig. 2 (b)), transient irreversible dynamics can occur, but these systems become point-reversible, loop-reversible, or steady-state irreversible as  $n \rightarrow \infty$ . Point-reversible systems tend to form ordered, size-segregated layers, in which particles cannot collide during simple shear. Further, the loop-reversible to irreversible transition in steady-state  $\phi_R(\gamma_{\max})$  is bounded in the large- $\gamma_{\max}$  limit by the highest packing fraction  $\phi_R$  at which systems can form ordered, size-segregated layers;  $\phi_I(\gamma_{\max} \rightarrow \infty) = \phi_R = \pi/4 \simeq 0.785$  in 2D and 0.605 in 3D in the  $N \rightarrow \infty$  limit.

In Fig. 2 (b), scatter plots of  $L(n)$  versus  $\Delta r_1(n)$  for 2D systems illustrate the evolution of the dynamics with increasing  $n$ . The points form several well-defined clusters: point-reversible ( $P$ ) with  $L < \tau_L$  and  $\Delta r_1 < \tau_r$ , loop-reversible ( $L$ ) with nonzero  $L$  ( $L > \tau_L$ ) and  $\Delta r_1 < \tau_r$ , and irreversible ( $I$ ) with nonzero  $L$  ( $L > \tau_L$ ) and  $\Delta r_1 > \tau_r$ . The  $P$ ,  $L$ , and  $I$  clusters are separated by more than 3 orders of magnitude in  $\Delta r_1$  or  $L$ . For region  $L$ , we also mandate  $L > 30\Delta r_1$  since systems with  $L < 30\Delta r_1$  typically relax to point-reversible states. We also enforce  $\Delta r_1 > 0.3\sigma_s$  to define region  $I$  since systems with  $\Delta r_1 < 0.3\sigma_s$  typically relax to point- or loop-reversible states. Systems that do not fall within the bounds defining regions  $P$ ,  $L$ , and  $I$  are categorized as transient irreversible ( $T$ ). As  $n$  increases, the fraction  $F_t$  of systems in the transient regime vanishes as a power-law  $n^{-\alpha}$  (where  $\alpha = 0.56 \pm 0.01$ ), while the fraction of point-reversible, loop-reversible, and steady-state irreversible systems saturates near  $10^4$  cycles (inset to Fig. 2 (b)).

We also characterized the dynamics of these systems as they approach steady-state point- and loop-reversible states (Fig. 3 (a)). We find that the single cycle mean-square displacement can be described by a function that interpolates between power-law and exponential decays at short and long times, respectively:

$$\Delta r_1^f(n) = f_+(n)(n/n_c)^{-\alpha} + f_-(n)e^{-\beta(n-n_c)}, \quad (5)$$

where  $f_{\pm}(n) = (1 + e^{\pm\bar{\gamma}(n-n_c)})^{-1}$ ,  $\bar{\gamma} \sim 1$ ,  $n_c$  is the cycle number at which the decay changes from power-law to exponential behavior,  $\alpha$  is a power-law scaling exponent, and  $\beta$  characterizes the exponential decay.

In Fig. 3 (b), we plot the best fit  $\Delta r_1^f(n)$  versus  $\Delta r_1(n)$  at each  $\gamma_{\max}$  and  $\phi$  (averaged over 16 initial conditions) for the 2D systems in Fig. 2 that evolve to point-reversible states. The scaling function in Eq. 5 collapses more than 60% of point-reversible systems with deviations  $\Delta = \langle (\log_{10} \Delta r_1^f(n) - \log_{10} \Delta r_1(n))^2 \rangle < 0.18$ . The top and bottom insets in Fig. 3 (b) show the power-law scaling and exponential decay of  $\Delta r_1(n)$  separately. We find similar scaling for the approach to loop-reversible states. However, the exponential decay for loop-reversible systems is difficult to differentiate from numerical error because the long-time dynamics occurs at larger  $n_c$  and smaller  $\Delta r_1$  than that for point-reversible systems. In Fig. 3 (c), we show the power-law decay for all systems that evolve to loop-reversible dynamical

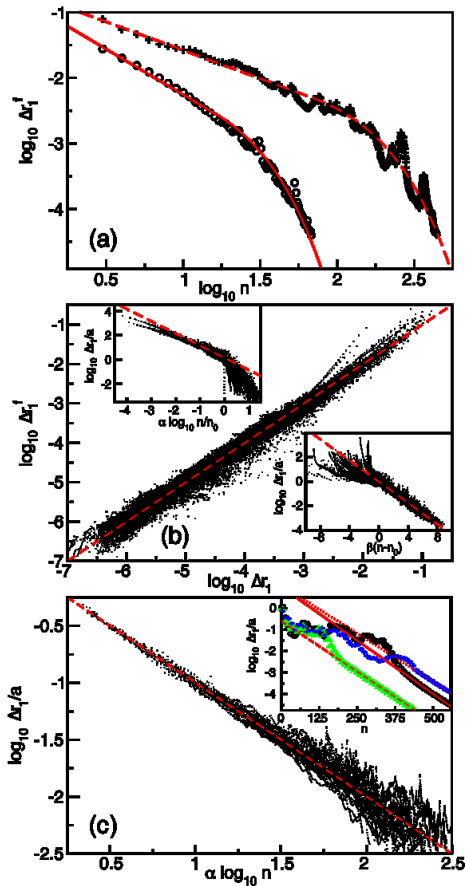


FIG. 3: (color online) (a) Single cycle mean-square displacement  $\Delta r_1$  versus  $n$  for a point-reversible system at  $\phi = 0.64$  and  $\gamma_{\max} = 0.5$  (circles) and a loop-reversible system at  $\phi = 0.8$  and  $\gamma_{\max} = 0.5$  (pluses) with best fits to  $\Delta r_1^f$  (Eq. 5) indicated by solid and dashed lines. (b) Comparison of  $\Delta r_1(n)$  (averaged over 16 initial conditions for each  $\gamma_{\max}$  and  $\phi$ ) to  $\Delta r_1^f(n)$  (black dots), where  $n$  is the cycle number, for point-reversible systems in Fig. 2 with  $\Delta < 0.18$ .  $\Delta r_1^f(n) = \Delta r_1(n)$  is indicated by the dashed line. The top left inset shows  $\log_{10} \Delta r_1(n)/a$  versus  $\alpha \log_{10} n/n_c$  (black dots). The dashed line indicates  $\Delta r_1(n)/a = (n/n_c)^{-\alpha}$ . The bottom right inset shows  $\log_{10} \Delta r_1(n)/a$  versus  $\beta(n - n_c)$  (black dots).  $\Delta r_1(n)/a = e^{-\beta(n - n_c)}$  is indicated by the dashed line. (c)  $\log_{10} \Delta r_1(n)/a$  versus  $\alpha \log_{10} n$  (black dots) for systems in Fig. 2 that evolve to loop-reversible dynamical states with  $\Delta < 0.04$ .  $\Delta r_1(n)/a = n^{-\alpha}$  is indicated by the dashed line. The inset shows  $\Delta r_1/a$  versus  $n$  for three independent initial conditions (squares, triangles, and pluses) at  $\phi = 0.76$  and  $\gamma_{\max} = 0.8$ . Exponential fits to the large  $n$  regime are shown as solid, dashed, and dotted lines with slopes  $\beta = 0.029, 0.026$ , and  $0.016$ , respectively.

states. In the inset, we also show several systems for which we captured the long-time exponential decay.

In Fig. 4 (a), we show the power-law scaling exponent  $\alpha$  for 2D systems that evolve to point- and loop-reversible states versus  $\phi$  and  $\gamma_{\max}$ . We find that  $\alpha \lesssim 1$  for all loop-reversible systems and point-reversible systems near the

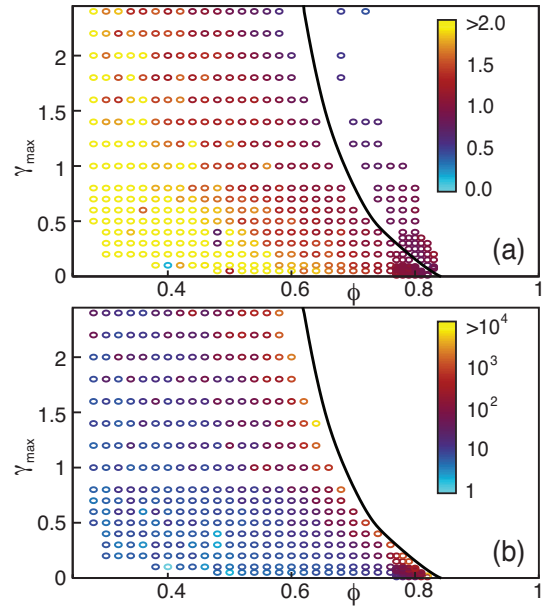


FIG. 4: (color online) (a) Contour plot of the power-law exponent  $\alpha$  (Eq. 5) versus  $\phi$  and  $\gamma_{\max}$  for 2D systems that evolve to either point- (circles) or loop-reversible (crosses) states. (b) Contour plot of the cycle number  $n_c$  (Eq. 5) that controls the crossover from power-law to exponential decay versus  $\phi$  and  $\gamma_{\max}$  for the point-reversible systems in (a).

crossover from point- to loop-reversible behavior, which suggests that the origin of the slow dynamics is related to contact or “collision” percolation. In contrast,  $\alpha > 1$  for point-reversible systems at low  $\phi$  and  $\gamma_{\max}$ . In Fig. 4 (b), we plot  $n_c$  for point-reversible systems versus  $\phi$  and  $\gamma_{\max}$ . We find that  $n_c$  increases with  $\phi$  and  $\gamma_{\max}$ , and appears to be diverging as the system approaches the transition from point- to loop-reversibility.

To test the stability of steady-state loop-reversible states, we perturb all particles at strain  $\gamma = 0$  by an amplitude  $\delta$  in random directions [14]. We then perform cyclic simple shear on the perturbed system and measure the deviation,  $\Delta_r = \sqrt{(N\sigma_s^2)^{-1} \sum_i |\vec{r}_{n,0}^i - \vec{r}_{n,0}^{i,p}|^2}$ , where  $\vec{r}_{n,0}^{i,p}$  are the coordinates of the perturbed system after  $t$  cycles required to reach steady state at each  $\phi$  and  $\gamma_{\max}$ . We find that loop-reversible systems are stable ( $\Delta_r < \tau_r$ ) for perturbations  $\delta < \delta_c \simeq 10^{-1}$ , *i.e.* perturbations as large as one-tenth of a particle diameter, where  $\delta_c$  is relatively insensitive to  $\phi$  for  $\gamma_{\max} \lesssim 1$ .

In conclusion, we studied the extent to which particle-scale motion can be reversible in athermal systems undergoing cyclic quasistatic loading. We identified two types of reversible behavior. For point-reversible states, particles do not collide and therefore trivially retrace their paths. For loop-reversible states, all particles undergo multiple collisions and have complex trajectories, yet all particles return to the locations they were in at the beginning of the cycle. We determined the regions of packing

fraction and strain amplitudes in 2D and 3D where these dynamical states are stable. In particular, we find that loop-reversible states occur over a range of packing fraction from contact percolation [10] to jamming onset, and thus our results emphasize that complex spatiotemporal dynamics are found well below  $\phi_J$ . Loop-reversible dynamical states represent a novel form of self-organization that will enable reliable preparation of configurations

with particular structural and rheological properties over a broad range of packing fractions.

We acknowledge support from NSF grant numbers NSF MRSEC DMR-1119826 (CS), DMR-1006537 (RH), CBET-0968013 (MS), and CBET-0967262 (CO). We also thank S. Papanikolaou, S. S. Ashwin, and T. Bertrand for helpful discussions.

- 
- [1] P. Schall, D. A. Weitz, and F. Spaepen, *Science* **318** (2007) 1895.
  - [2] J. S. Harmon, M. D. Demetriou, W. L. Johnson, and K. Samwer, *Phys. Rev. Lett.* **99** (2007) 135502.
  - [3] M. L. Falk and J. S. Langer, *Ann. Rev. Condens. Matter Physics* **2** (2011) 353.
  - [4] M. Nicolas, P. Duru, and O. Pouliquen, *Eur. Phys. J. E* **3** (2000) 309.
  - [5] E. R. Nowak, J. B. Knight, E. Ben-Naim, H. M. Jaeger, and S. R. Nagel, *Phys. Rev. E* **57** (1998) 1971.
  - [6] M. Lundberg, K. Krishan, N. Xu, C. S. O'Hern, and M. Dennin, *Phys. Rev. E* **77** (2008) 041505.
  - [7] D. J. Pine, J. P. Gollub, J. F. Brady, and A. M. Leshansky, *Nature* **438** (2005) 997.
  - [8] Laurent Corte, P. M. Chaikin, J. P. Gollub, and D. J. Pine, *Nature Physics* **4** (2008) 420.
  - [9] S. Slotterback, M. Mailman, K. Ronaszegi, M. van Hecke, M. Girvan, and W. Losert, *Phys. Rev. E* **85** (2012) 021309.
  - [10] T. Shen, C. S. O'Hern, and M. D. Shattuck, *Phys. Rev. E* **85** (2012) 011308.
  - [11] M. P. Allen and D. J. Tildesley, *Computer Simulation of Liquids* (Oxford University Press, New York, 1987).
  - [12] G.-J. Gao, J. Blawdziewicz, and C. S. O'Hern, *Phys. Rev. E* **80** (2009) 061303.
  - [13] N. Xu and C. S. O'Hern, *Phys. Rev. Lett.* **94** (2005) 055701.
  - [14] See Supplementary Materials, which include results for 2D and 3D systems as a function of system size  $N$ , shear strain increment  $\Delta\gamma$ , and energy minimization threshold  $V_{th}$ .